https://doi.org/10.1016/j.jhazmat.2021.125483

Evolution of Redox Activity of Biochar during Interaction with Soil Minerals: Effect on the Electron Donating and Mediating Capacities for Cr(VI) Reduction

Zibo Xu[a,b], Xiaoyun Xu[a*], Yulu Yu[a], Chengbo Yao[c], Daniel C.W. Tsang[b*], Xinde Cao[a,d]

[a] School of Environmental Science and Engineering, Shanghai Jiao Tong University, Shanghai 200240, China

[b] Department of Civil and Environmental Engineering, The Hong Kong Polytechnic University, Hung Hom, Kowloon, Hong Kong, China

[c] Department of Chemistry, Columbia University, 3000 Broadway, New York, New York 10027, United States

[d] Shanghai Institute of Pollution Control and Ecological Security, Shanghai 200092, China

Corresponding author: E-mail: xuxiaoyun@sjtu.edu.cn; dan.tsang@polyu.edu.hk.

Abstract

Biochar in soil is susceptible to natural aging along with soil minerals, which might alter its electrochemical properties and redox reactions with contaminants. In this study, soluble mineral salts ($FeCl_3$, $MnCl_2$, $AlCl_3$, $CaCl_2$) and clay mineral (kaolinite) were selected to investigate the impact of co-aging with soil minerals on the redox activity of peanut-shell biochar for Cr(VI) reduction. Natural aging for 3-month induced oxidation of biochar with the decrease of reducing moieties, i.e., -C-OH from 26.8-43.7% to 18.4-24.1%. Co-aging with minerals except for Mn(II) further decreased the proportion of -C-OH to 6.94-22.2% because of the interaction between mineral ions and biochar, resulting in the formation of mineral-biochar complex and new minerals, e.g. β-FeOOH. Due to its reductivity, Mn(II) presented the least decrease or even slight increase of-C-OH while itself was oxidized to Mn(III) and Mn(IV). The decline of -C-OH caused the decrease of Cr(VI) reduction rate constant from 2.18-2.47×10^{-2} h^{-1} for original biochars to 0.71-1.95×10^{-2} h^{-1} for aged ones, of which co-aging with Fe(III) showed the lowest reduction rate constant among all minerals. The electron mediating capacity of biochar also decreased after aging alone or co-aging with Al, Ca, and kaolinite, while co-aging with Fe(III) and Mn(II) facilitated the electron transfer process, increasing the rate constant by 219.3-1237% due to electron mediation through valence transformation of Fe(III)-Fe(II) and Mn(II)-Mn(III). Given the abundance of soil minerals, it was essential to consider this crucial factor for redox reactions when applying biochar for soil remediation.

Keywords: Biochar aging; Chromium; Electron transfer; Soil minerals; Sustainable remediation.

28**Graphical Abstract**

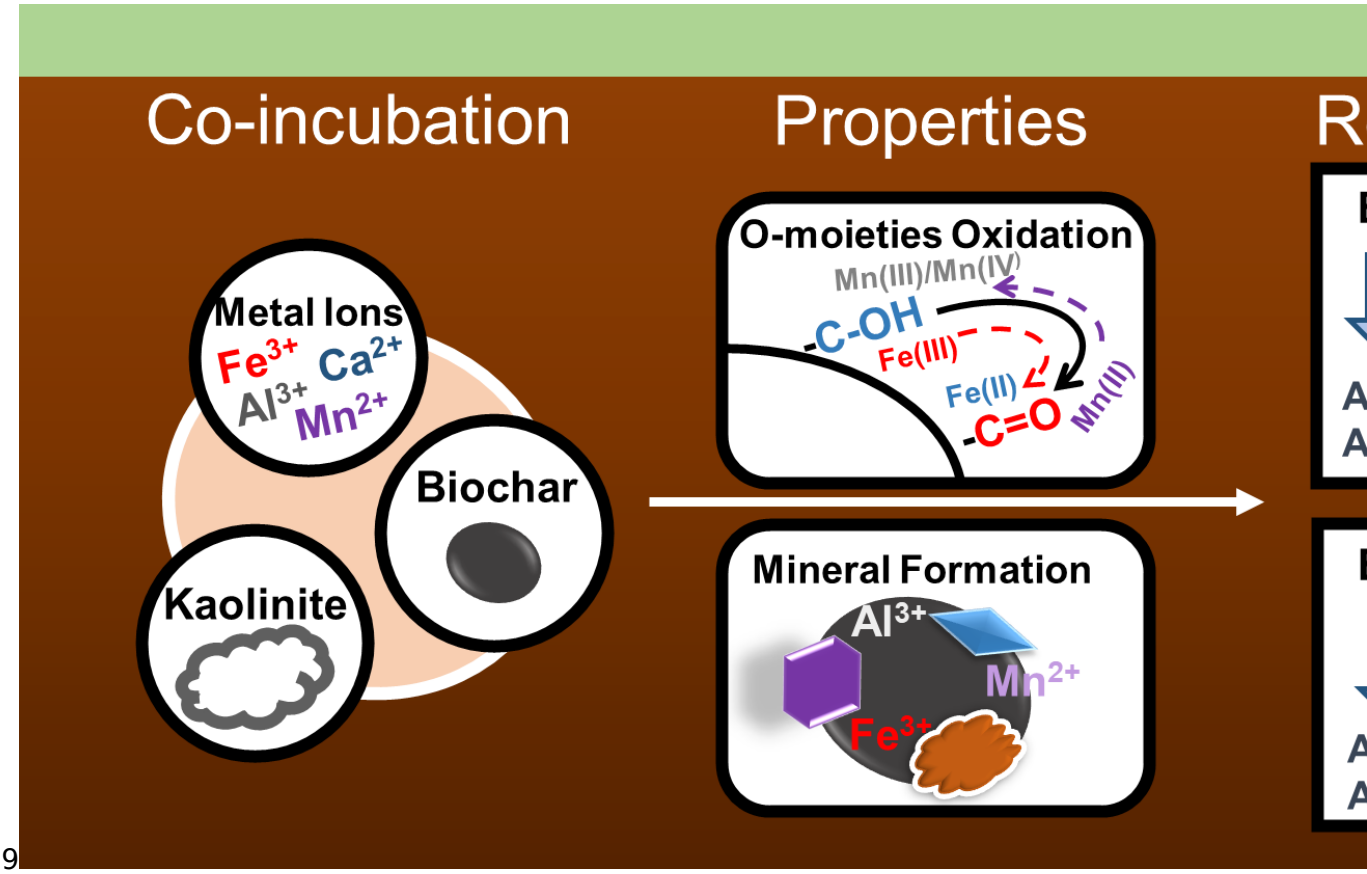

1. Introduction

Biochar is a carbonaceous residue which comes from incomplete combustion of biomass in the absence of oxygen (Lehmann 2007, Zhao et al. 2013). It has been widely recognized that biochar in soil has multi-functions including carbon sequestration (Schmidt et al. 2019), nutrient availability enhancement (Rafique et al. 2020), plant growth facilitation (Hussain et al. 2017), and contaminant immobilization (Cao and Harris 2010, Qi et al. 2017). Recently, potential of biochar as a redox-active material for pollutant control has been unveiled. The electron donating, electron accepting, and electron mediating capacities of biochar could contribute to, or even determine, the degradation of organic pollutants and the reductive/oxidative-immobilization of metals/metalloids (Chen et al. 2019, Liu et al. 2020, Qiu et al. 2020, Sun et al. 2019, Tu et al. 2020).

A prerequisite for the successful application of biochar as a redox-active material

for soil pollution control is that its redox activity maintains over a long period of time (Ren et al. 2018). However, it has been revealed that the physicochemical properties of biochar including alkalinity (Mukherjee et al. 2014), surface O-containing moieties (Ghaffar et al. 2015), mineral components (Xu et al. 2018b), and surface area (Zhao and Zhou 2019) would be altered during aging process. Therefore, many published studies reported the variation of the sorption capacity of aged biochar for metals/metalloids and organic pollutants (Deng et al. 2020, Huang et al. 2020, Tan et al. 2020, Wang et al. 2020). Since natural aging in soil was mostly similar to an oxidation process (Mia et al. 2017, Wang et al. 2020), the redox activity of biochar for pollutant immobilization might also be susceptible to aging. The alternation of O-containing moieties, surface properties, and carbon structures during aging process would affect the electron donating and accepting capacities of biochar (Li et al. 2020, Qin et al. 2020). Besides, the electron mediating capacity of biochar might also be influenced because the electron shuttling mainly depended on the cyclic transformation of surface O-containing moieties or conjugated carbon structures of biochar (Sun et al. 2017, Wan et al. 2020, Xu et al. 2020b). It can be speculated that the pollutant immobilization through both direct electron exchange (donating and accepting) and electron mediation by biochar would be changed during aging, while our understanding about the impact of aging on this process was still limited.

Soil minerals, which occupy almost half of soil constituent, might also participate in the aging process of biochar, especially over a long period of time (Wang et al. 2013), and their interaction could further change the electrochemical properties of biochar, thus affecting its redox activity (Xu et al. 2020a). It has been reported that mineral particles could interact with the surface of biochar in the first few months after the application of biochar in the field soil (Lin et al. 2012), resulting

in the formation of organo-mineral phases (Archanjo et al. 2017). Moreover, minerals with redox activity, e.g. Fe/Mn minerals, could not only change the properties of biochar by both physical attachment and chemical redox reaction (Mumme et al. 2018, Yang et al. 2016), but also take part in the electron transfer process of biochar for pollutant immobilization, e.g., Cr(VI) (Xu et al. 2018a, Xu et al. 2020a). Our previous research found that Fe(III) minerals could oxidize the surface functional groups and decrease the reduction capacity of biochar, while Fe(III) could also facilitate the electron shuttling process due to the valence transformation of Fe(II)-Fe(III) (Xu et al. 2020a). It remains unclear how co-aging with different soil minerals affects the redox activity of biochar as well as the electron transfer process for pollutant immobilization.

In this study, we chose the reduction of Cr(VI) by biochar to represent the redox activity of biochar for soil pollutant immobilization since biochar could effectively reduce the highly toxic Cr(VI) to Cr(III) of low toxicity through both electron donating and electron shuttling mechanisms. Two pyrolysis temperatures, 400°C and 700°C, were selected to represent low and high temperature used for biochar production, respectively. Low temperature produced biochar mainly participate in the Cr(VI) reduction process with surface O-moiety while conjugated aromatic structure of high temperature biochar might play a key role during Cr(VI) reduction (Xu et al. 2020b, Sun et al. 2017). We hypothesized that the interactions between soil minerals and biochar would alter the redox activity of biochar during the aging process, and accordingly change the electron donating and electron shuttling capacities of biochar for Cr(VI) reduction. To test this hypothesis, this study was conducted (1) to determine changes in properties of peanut-shell biochar during the co-aging process with soluble mineral salts ($FeCl_3$, $MnCl_2$, $AlCl_3$, and $CaCl_2$) and clay mineral

(kaolinite); (2) to elucidate the changes of biochar's reducing and shuttling capacities for Cr(VI) reduction after aging; and (3) to explore the mechanisms of biochar aging with soil minerals on electron transfer during Cr(VI) reduction. It is worth mentioning that the electron donating and mediating capacity of biochar was measured in ideal aqueous system to exclude the impact of other soil moieties in this study.

2. Materials and Methods

2.1 Biochar and Minerals

The biochar used in this study was produced from peanut shell through a slow pyrolysis under N_2 atmosphere at 400°C or 700°C with heating rate of 10°C min^{-1} and a holding time of 4 h. Peanut shell was selected as the feedstock for biochar preparation due to the highest reducing capacity of produced biochar according to our previous research (Xu et al. 2019a, Zhang et al. 2018). Detailed production procedure has been described previously (Zhao et al. 2013). The biochar produced at 400°C and 700°C was referred to BC400 and BC700, respectively. The resulted biochars were then grounded by ball-milling (QM-3SP04, China) at 150rpm for 4h, and passed through a 200-mesh (0.074 mm) sieve. Basic properties of biochar including element content, carbon structure, electro-chemical properties, and surface functional group was characterized and presented in Table S1 (detailed procedures were described in Supporting Information). Electro-chemical properties of biochar (i.e. electron donating capacity and electron accepting capacity) were quantified by mediated electrochemical reduction (MER) and oxidation (MEO) test (Zhang et al. 2018, Zhang et al. 2019) (detailed procedure could be found in Supporting Information).

Four typical widespread soil soluble mineral salts including aluminum chloride ($AlCl_3$), iron chloride ($FeCl_3$), manganese chloride ($MnCl_2$), calcium chloride ($CaCl_2$), and one clay mineral kaolinite ($Al_2O_3 \cdot 2SiO_2 \cdot 2H_2O$) were selected for the incubation experiment (Yang et al. 2016). Kaolinite was one of the main clay minerals in soil and it might stimulate the Cr(VI) reduction with organic carbon and redox active metal ions (Kwak et al. 2018, Buerge and Hug 1999, Deng et al. 2003). Redox active Fe^{3+} and Mn^{2+} as chlorides were chosen to simulate the metal ions dissolved from Fe/Mn (hydr)oxides or released from non-clay minerals in soil. Al^{3+} and Ca^{2+} as chlorides were chosen as the commonly found non-redox active cations. Soluble mineral salts were selected in this study since they had higher impact on biochars' redox activity than solid minerals (e.g. (hydr)oxide) (Xu et al. 2020a).

2.2 Co-aging of biochar with minerals

Biochar samples were heated at 100°C to degas volatile organic carbons prior to aging (Xu et al. 2018b). Simulation of natural aging was performed by incubation with 70% MWHC (Maximum Water Holding Capacity) in dark for 15 days and 3 months (Guo et al. 2014). The moisture content was selected according to the soil moisture content (Cao et al. 2011), and maintained by adding deionized water to compensate water loss every other day. The incubation experiment was conducted in glass containers (71 mm in internal diameter and 97 mm in height) with 10 different arrangements: (1) 10 g biochar alone; (2–5) 10 mM $FeCl_3$, $MnCl_2$, $AlCl_3$, or $CaCl_2$ mixed with 10 g biochar, respectively; (6) 10 g biochar mixed with 10 g kaolinite; and (7–10) 10 mM $FeCl_3$, $MnCl_2$, $AlCl_3$, or $CaCl_2$ mixed with 10 g biochar and 10 g

kaolinite. Concentration of soluble metal ions was set according to the appropriate proportion of biochar and the range of metal contents in soil (Yu et al. 2020, Zhao et al. 2007). The dosages of the metal chlorides were about 2.7-5.6% (w/w) of kaolinite on the basis of metal elements, which could represent real environmental conditions (Li et al. 2013, Yang et al. 2016). Experimental setting 1 was used to identify the effect of aging process alone, and experimental settings 2-5 were used to clarify the role of soluble mineral ions during the aging process. Kaolinite was added into experimental settings 6-10 in order to simulate the existence of clay mineral in natural soil. All these samples were collected after 15 days and 3 months aging, then air-dried and stored in an airtight container.

2.3 Characterization of biochar-mineral interaction during aging process

In order to determine the possible mineral formation on the biochar during the aging process, the aged biochar particles were characterized by X-ray diffraction (XRD) (D/max-2200/PC, Japan Rigaku Corporation) and the data was collected over the 2θ range from 10° to 70° with a scan speed of 3° min^{-1}. X-ray photoelectron spectroscopy (XPS, PHI 5000, ULVAC-PHI) was conducted to provide semi-quantification analysis for the changes of surface functional groups on biochar upon the aging process (Arrigo et al. 2010, Singh et al.2014, Zhao et al. 2021). Transition of surface functional groups is also complemented by Fourier transform infrared spectroscopy (FTIR) (IR Prestige 21 FTIR, Shimadzu, Japan). Besides, the species of mineral on selected group of aged biochar was also measured by XPS in order to determine the change of valence state on biochar during the aging process and

detailed XPS peak position were shown in Supporting Information. Scanning electron microscope (SEM) with energy dispersive spectrometer (EDS) was used to determine the morphology and chemical composition of any attached minerals and biochar particles.

2.4 Direct electron donating capacity for Cr(VI) reduction by aged biochar

The kinetics experiment was conducted to determine the direct reduction kinetics of Cr(VI) by aged biochar. Specifically, 2 g (dry weight) fresh or aged biochar particles were added into 1 L of 50 mg L^{-1} Cr(VI) solution. The stock solution of 50 mg L^{-1} Cr(VI) was prepared by dissolving an appropriate amount of K_2CrO_4 in 0.1 M KCl solution. High ionic strength was used to keep the ionic strength during the reduction process. The pH values were kept at 3 by potassium hydrogen phthalate ($C_8H_8KO_4$) buffer solution (Kwak et al. 2018). Low pH was selected to achieve relatively high Cr(VI) reduction rate, thus shortening the reaction time (Kwak et al 2018, Wan et al. 2019). The buffering agent will not participate in the Cr(VI) reduction process with biochar (Xu et al. 2020a). The mixtures were mechanically agitated at 140 rpm on a reciprocating shaker at 25°C for 48 h and sampled at selected time intervals. Total Cr concentration and Cr(VI) concentration were determined by ICP-OES (Agilent 5110, USA) and diphenyl-carbohydrazide spectrophotometric method, respectively. Cr(III) concentration was calculated by the difference between the total Cr and Cr(VI) concentrations. Detailed sampling and characterization methods including Cr(VI), Cr(III), total Cr (Cr(Total)) concentration, and other metals concentrations for the filtrates were described in Supporting Information. Pseudo

first-order model was used to fit the rate constant of Cr(VI) reduction by aged biochar and detailed calculation methods were described in Supporting Information. The aged biochar (3-month aging with Fe(III) or Mn(II)) were characterized for C, O, Fe/Mn, and Cr species by XPS after Cr(VI) reduction, and detailed peak positions could be found in Supporting Information. SEM-EDS was also used to determine the Cr distribution on the biochar-mineral complex after reduction.

2.5 Electron mediating capacity for Cr(VI) reduction by aged biochar

The mediating capacity of biochar and aged biochar was determined in the reduction of Cr(VI) with lactate, which was a weak electron donor and representative naturally occurring organic acids in the soil environment (Xu et al. 2019b, Xu et al. 2020b). Specifically, 5 mM lactate and 2 g (dry weight) fresh or aged biochar particles were mixed with 1 L of 50 mg L^{-1} Cr(VI) stock solution. Lactate concentration (5 mM) was set on the basis of possible concentration in natural soil solution (Jones 1998, Krishnamurti et al. 1997, Xu et al. 2019b). Details of sampling and characterization methods were similar to the Section 2.4 and described in Supporting Information. Mediated reduction rate for aged biochar was also calculated using pseudo first-order model (Supporting Information).

3. Results and Discussion

3.1 Evolution of O-moieties on the surface of biochar during the aging process

Significant change of the surface functional groups on biochar was found during the aging process. The surface O/C ratio measured by XPS increased from 0.13-0.14

to 0.15-0.20 after biochar aging alone (Table S1 and S2), indicating the oxidization of biochar and formation of surface O-containing functional groups. According to the XPS spectra of O1s, the O-containing functional groups were divided into four species, including –C-OH, –C-O-C, –O-C=O, and quinonyl -C=O (Arrigo et al. 2010). Before aging, 43.7% and 26.8% of O-moieties on the biochar surface was –C-OH for BC400 and BC700, respectively (Fig. 1, Table S2, and Fig. S1&2). The high –C-OH content was proved to be responsible for the high reducing ability of biochar (Mandal et al. 2017, Zhang et al. 2018). The 3-month aging process decreased the –C-OH content to 17.0-24.1% and accordingly increased the contents of –C-O-C and –O-C=O (Fig. 1 and Fig. S1&2). The reductive –C-OH was transformed to the oxidative –O-C=O through the oxidation by O_2 during the aging process (Equation 1).

$$4(\text{–C-OH}) + 3O_2 \rightarrow 4(\text{–O-C=O}) + 2H_2O \qquad \text{Equation 1}$$

Soil mineral ions altered the O-moieties on biochar surface in distinctive ways during the aging process. Co-aging with Fe(III) facilitated the oxidization of biochar, which further decreased the –C-OH content to 6.94-12.5% (Fig. 1). Besides, quinonyl –C=O was newly formed after co-aging with Fe(III) (Fig. 1). The decrease of –C-OH and formation of quinonyl –C=O might be attributed to the oxidization of biochar by Fe(III) as shown in the equations 2-3. This redox process was further confirmed by the FTIR analysis which showed an increase of -COO with decrease of C-OH after reaction with Fe(III) (Fig.S3). Notably, 39.3-59.8% of Fe(II) was detected on the biochar surface by XPS (Fig. 2), confirming the reduction of Fe(III) by biochar during the aging process.

$$H_2O + –C\text{-}OH + 3Fe^{3+} \rightarrow –O\text{-}C{=}O + 3Fe^{2+} + 3H^{+} \quad \text{Equation 2}$$

$$–C\text{-}OH + Fe^{3+} \rightarrow –C{=}O + Fe^{2+} + H^{+} \quad \text{Equation 3}$$

By contrast, the addition of Mn(II) caused a slight rise of –C-OH content compared to the biochar aging alone, which increased from 17.0-18.4% to 21.2-22.2% after 3-month aging (Fig.1 and detailed data could be found in Table S2). Reduction ability of Mn(II) might be the main reason for the increase of reductive O-moieties as shown in the equations 4-5. This was verified by the appearance of both Mn(III) (25.3-29.7%) and Mn(IV) (11.9-20.2%) on the biochar surface after the aging process (Fig. 2).

$$2\,H^{+} + –O\text{-}C{=}O + 2\,Mn^{2+} \rightarrow –C\text{-}OH + 2\,Mn^{3+} + H_2O \quad \text{Equation 4}$$

$$2\,H^{+} + –O\text{-}C{=}O + 2\,Mn^{3+} \rightarrow –C\text{-}OH + 2\,Mn^{4+} + H_2O \quad \text{Equation 5}$$

Calcium without redox activity showed less change on the surface O-moieties of biochar (Fig. 1, Table S2, and Fig. S1-S2), with –C-OH content changing from 17.0-18.4% for biochar aged alone to 14.4-16.5% after 3-month aging. Interestingly, we found that Al caused a decline of –C-OH content to 15.9% and 9.17% for BC400 and BC700 after 3-month aging, respectively, meanwhile 8.49-8.96% of quinonyl –C=O was newly formed (Fig.1, Table S2, and Fig.S1-S2). Acidity from the hydrolysis of Al^{3+} might facilitate the oxidation process during the aging process (Equation 6). Rechberger et al. (2017) demonstrated that the oxidation of biochar incubated in acidic soil was more pronounced in comparison to that in mild soil. Similarly, Fe^{3+} could also be hydrolyzed with the formation of H^{+} and its hydrolysis might be even stronger than Al with a higher induced acidity (Yu et al. 2016), which also contribute

to the strong oxidation of biochar with Fe(III) (Equation 7).

$$3H_2O + Al^{3+} \rightarrow 3H^+ + Al(OH)_3 \quad \text{Equation 6}$$

$$3H_2O + Fe^{3+} \rightarrow 3H^+ + Fe(OH)_3 \quad \text{Equation 7}$$

3.2 Formation of new minerals and biochar-mineral complexes during the aging process

Interactions with soil minerals might not only change O-moieties of biochar, but also induce the formation of new minerals and biochar-mineral complexes. Crystalline quartz (SiO_2) and sylvite (KCl) could be detected in all aged biochars by XRD analysis. Quartz and sylvite were the inherent minerals of peanut-shell biochar which kept stable during the aging process (Xu et al. 2019b). Co-aging with different soluble mineral salts caused the formation of corresponding minerals (Fig. 3). Co-aging with Fe(III) formed poor crystalline akaganeite (β-FeOOH) due to the presence of Cl^- in the system (Sigg and Stumm 1981). In addition to the crystal iron mineral, amorphous iron mineral and sorbed iron ions might also be formed on the biochar surface due to the higher proportion of Fe(II) (39.3-59.8%) as detected by XPS analysis (Fig.2). More Fe(II) was formed on BC400 (45.2-59.8%) compared to BC700 (39.3-39.6%), due to the higher electron donating capacity (EDC, 1.55 mmol $e^-\cdot g^{-1}$ BC400 > 0.98 mmol $e^-\cdot g^{-1}$ BC700) caused by the higher reductive surface functionality (e.g. hydroxyl) at low pyrolysis temperature (Zhang et al. 2018). A series of new Mn minerals, including scacchite ($MnCl_2$), rhodochrosite ($MnCO_3$), potassium manganese oxide (K_2MnO_3), and groutite (MnOOH) with different valence states from +2 to +4 were formed on the biochar surface after co-aging with Mn(II).

Transition of Mn valence state was confirmed by XPS analysis (Fig. 2) that 25.3-29.7% of Mn(III) and 11.9-20.2% of Mn(IV) was formed on biochar surface after co-aging with Mn(II). It has been reported that Mn(II) oxidation with oxygen or other electron accepting moieties can be catalyzed on the surface of particles (e.g. biochar) and then precipitated as (oxyhydr)oxides of Mn(III) and Mn(IV) (Luo et al. 2020, Inoué et al. 2019). Higher content of Mn(IV) was found on BC700 (15.3-20.2%) compared with BC400 (11.8-17.8%) which might be attributed to the relatively higher alkalinity (Xiao et al. 2018) and higher oxidating capacity (i.e. electron accepting capacity, 1.07 mmol $e^{-}\cdot g^{-1}$ BC700 > 0.73 mmol $e^{-}\cdot g^{-1}$ BC400) (Table S1) caused by the surface carboxyl and quinolyl functional group (Zhang et al. 2019). Boehmite (AlOOH) and calcite ($CaCO_3$) were detected on the BC700 aged with Al and Ca, respectively, while limited Al minerals can be found on BC400 after aging with Al. Moreover, similar new minerals of Fe, Al, Ca, or Mn were formed on the corresponding aged biochars in experimental setting 6-10 with the presence of kaolinite (Fig. S4).

SEM elemental mapping revealed the attachment of minerals on the aged biochar. As shown in Fig. S5&6, all mineral ions could be adsorbed on the biochar surface and possibly formed the biochar-mineral complexes after 3-month incubation with assistance of the carboxylic functional groups on biochar (Lin et al. 2012). Some crystal minerals were found tightly attached on the biochar surface in Fig. S5b, which confirmed the formation of new minerals and the association of minerals with biochar. This phenomenon might be common in soil after the biochar application (Zhao and

292Zhou 2019).

293 In conclusion, both alteration of O-moieties and formation of new minerals as
294well as biochar-mineral complexes were observed during the biochar aging with soil
295minerals, which would affect the redox activities of biochar for the direct or mediated
296Cr(VI) reduction.

297*3.3 Changes in the reducing capacity of biochar for Cr(VI) reduction after the aging*
298*process*

299 Fresh BC400 and BC700 decreased the solution Cr(VI) concentrations from
30050.0 mg L^{-1} to 10.1-12.3 mg L^{-1} after 48-h reaction, and the Cr(III) concentration
301increased to 28.4-35.8 mg L^{-1} (Fig. S7) in the meantime. Aging process compromised
302the Cr(VI) reduction efficiency of biochar and up to 32.7 mg L^{-1} Cr(VI) was still left
303in the solution (Fig. S8-S16). Over 78.2% of total Cr on the aged biochar was Cr(III)
304after Cr(VI) reduction (Fig. S17) and spherical particles were formed on the biochar
305surface (Fig. S18), which indicated possible formation of Cr(III) crystal minerals.
306Previous study reported the formation of CrOOH after the reduction of Cr(VI) by
307peanut-shell biochar (Xu et al. 2019a). All these results confirmed that reduction was
308the main mechanism for the immobilization of Cr(VI) by biochar even after the 3-
309month aging with minerals.

310 Aging process of biochar alone lowered the Cr(VI) reduction rate constants from
3112.18 × 10^{-2} h^{-1} to 0.96-1.22 × 10^{-2} h^{-1} for BC400 and from 2.47 × 10^{-2} h^{-1} to 1.28-1.95 ×
312$10^{-2}$ h^{-1} for BC700 (Fig. 5 and Table S3-S4). This was probably due to the decrease of
313reductive C-OH (Rajapaksha et al. 2018, Xu et al. 2019b, Xu et al. 2020b). Besides,

fast decay of the persistent free radicals with interaction with oxygen (Gehling and Dellinger 2013, Odinga et al. 2020) might also contribute to the decrease of reduction rate since it could directly participated in Cr(VI) reduction (e.g. O-centered radicals and C-centered radicals) (Xu et al. 2019a, Zhong et al. 2018). With the participation of mineral ions, the change of Cr(VI) reduction rate varied with the types of both mineral ions and biochar. For BC400, aging with Fe(III) further lowered the reduction rate constant from 1.22 × 10^{-2} h^{-1} for biochar aged alone to 1.02 × 10^{-2} h^{-1} after 15-day incubation. The reduction rate of biochar aged with Fe(III) barely changed with the increasing time from 15-day to 3-month incubation (Fig. 4 and Table S3), which was similarly observed for the other minerals, indicating fast interactions between mineral ions and biochar within 15 days. Compared to biochar aged alone, other mineral ions increased the reduction rate constants of aged biochar from 0.96 × 10^{-2} h^{-1} to 1.18-1.23 ×10^{-2} h^{-1} after 3-month aging (Fig. 4 and Fig. S7-9). However, for BC700, all mineral ions caused an obvious decrease of reduction rate constants from 1.28-1.95 × 10^{-2} h^{-1} to 0.71-1.13 × 10^{-2} h^{-1} compared to the aging process without mineral ions (Fig. 4 and Table S4). Similar to BC400 system, Fe(III) showed the most significant decrease of reduction rate constants from 1.28 ×10^{-2} h^{-1} of BC700 aged alone to 0.71 ×10^{-2} h^{-1} after 3-month aging. The change in reduction rates of BC700 was much more significant than that of BC400 during the aging process, probably because the higher surface area offered the reaction interface with mineral cations (Xu et al. 2020a).

The most decrease of reduction rates in biochar aged with Fe(III) might be explained by two main reasons. First one was the highest decrease of –C-OH during

the aging process (Fig. 1). A linear correlation (Fig. 5a, b) between the –C-OH content and reduction rate constants was found on both BC400 and BC700 (R^2=0.62-0.72), indicating that –C-OH was the key reducing moiety on the biochar surface for Cr(VI) reduction. The decrease of –C-OH content from 12.4-21.2% to 10.3-18.3% and from 8.08-22.1% to 4.62-15.4% after Cr(VI) reduction by 3-month aged BC400+Fe(III) and BC700+Fe(III), respectively (Fig. 6c, d, S19 and Table S5), confirming the importance of –C-OH in the redox activity of biochar. Another reason might be the formation of Fe(II) during the aging process. As shown in Fig. 2, 39.3-59.8% of Fe(II) was formed on biochar surface after aging, and 38.1-35.7% of Fe(II) still remained after Cr(VI) reduction. Electrons from the biochar could be captured by Fe(III) to form Fe(II) and rendered unavailable for Cr(VI) reduction. Reduction of Cr(VI) by the Fe(II) sorbed on the biochar surface would be blocked due to the cover of new formed precipitates (e.g. Fe(III) precipitates or Fe(III)-Cr(III) co-precipitate) on biochar surface (Bishop et al. 2019, Nelson et al. 2019). The decrease of electron donating amount of biochar for Cr(VI) reduction would be associated with the decrease of reduction rate (Xu et al. 2020a).

The smaller decrease of Cr(VI) reduction rates for BC400 co-aged with other mineral ions (Ca, Al, Mn), compared to BC400 aged alone, was partly related to the less significant decrease of –C-OH content during the aging process, especially for biochar co-aged with Mn (Fig. 1). More importantly, free mineral ions with positive charge might bind with negative surface functional groups (e.g. –C-O^-) to form –C-OM^{n+} (e.g. –C-OCa^+) on BC400, and thus facilitate the electron transfer from the

negatively-charged biochar surface to the Cr(VI) via cation bridging (Han et al. 2016, Yang et al. 2018). As shown in Fig. S20, the distribution of Cr was overlapped with soil mineral ions (Al and Ca) on the biochar surface, probably due to the complexation of chromate with mineral ions, immobilization of Cr on newly formed minerals (Shi et al. 2020), or co-precipitation into new minerals (Mullet et al. 2007). This may serve as circumstantial evidence for the participation of mineral ions in the interactions between biochar and Cr(VI). However, it is worth noting that the negative effect of a greater decrease of –C-OH content after co-aging with Fe(III) might overwhelm the positive effect of cation bridging, thus lowering the Cr(VI) reduction rate as compared to BC400 aged alone (Fig. 4c). For BC700 with much less surface O-containing functional groups (Table S1), the positive effect of cation bridging might be too limited to increase the reduction rate for BC700 co-aged with mineral ions (Fig. 5b). Therefore, the negative effect of more significant –C-OH decrease determined the higher decrease of reduction rates of BC700 co-aged with mineral ions than BC700 aged alone (Fig.5b).

After 3-month co-aging with kaolinite, the reduction rate constants increased from $0.96 \times 10^{-2}\ h^{-1}$ to $1.33 \times 10^{-2}\ h^{-1}$ for BC400 and from $1.28 \times 10^{-2}\ h^{-1}$ to $1.58 \times 10^{-2}\ h^{-1}$ for BC700, respectively, compared with biochar aged alone (Fig. 5 and Table S3-S4). Although kaolinite showed marginal redox activity, interaction happened on the interface between biochar and kaolinite might preserve the redox activity of biochar, because the formed biochar-kaolinite complex (as shown in Fig. S21) had relatively higher stability (Yang et al. 2018, Yang et al. 2016). However, in the presence of

mineral ions, the reduction rate constants decreased to 0.99-1.10 $\times 10^{-2}$ h^{-1} for BC400 and 0.67-1.13 $\times 10^{-2}$ h^{-1} for BC700, respectively, compared with biochar aged with kaolinite alone (experimental setting 6-10) (Fig. 5c, d and Table S3-S4). This might be related to the more significant decrease in –C-OH content during the aging process. Besides, mineral ions could be sorbed by kaolinite (Turan et al. 2007, Zhu et al. 2018), which resulted in the decline of metal concentrations in solution (Fig. S8-S11 vs Fig. S13-S16) and hindered the positive effect of cation bridging.

3.4 Alteration of the mediating capacity of biochar for Cr(VI) reduction after the aging process

Lactate, a weak electron donor, could hardly reduce the Cr(VI) in solution according to the previous study (Xu et al. 2020b). However, the reduction amount of Cr(VI) by biochar with lactate (Fig.S22) was much higher than the one by biochar alone (Fig.4), which probably suggested the shuttling effect of biochar (Table S3-S4). The gap between the rate constants of biochar alone and biochar with lactate was considered as the mediated reduction rate constants as shown in Fig. 6.

The aging process inhibited the electron mediation of biochar for Cr(VI) reduction and significantly decreased the mediated reduction rate constants from 3.91-5.82 $\times 10^{-3}$ h^{-1} to 1.46-2.13 $\times 10^{-3}$ h^{-1} (Fig. 6, and Table S3-S4). Surface functional groups (e.g. –C-OH) are considered as the main electron mediating moieties of biochar for Cr(VI) reduction (Xu et al. 2019a, Xu et al. 2020b), thus the decrease of the surface –C-OH group during the aging process might be the major reason for the decline of mediated reduction rate. Interestingly, the aging process with mineral ions

showed different effects on the mediating capacity of biochar. Compared with fresh biochar, co-aging with Fe(III) increased the mediated reduction rate constants from 3.91 $\times 10^{-3}\ h^{-1}$ to 22.3 $\times 10^{-3}\ h^{-1}$ and from 5.82 $\times 10^{-3}\ h^{-1}$ to 6.67$\times 10^{-3}\ h^{-1}$ for BC400 and BC700 after 15-day aging, respectively, and the reduction rate constants remained high after 3-month aging with Fe(III), as 20.4 $\times 10^{-3}\ h^{-1}$ and 6.80 $\times 10^{-3}\ h^{-1}$ for BC400 and BC700, respectively (Fig.6). Co-aging with Mn(II) similarly caused a significant increase of mediated reduction rate constants to 11.8-14.9 $\times 10^{-3}\ h^{-1}$ and 7.63-8.01 $\times 10^{-3}\ h^{-1}$ for BC400 and BC700, respectively. Compared with the biochar aged alone, aging with Fe(III) and Mn(II) apparently increased the rate constants by approximately 487-1237% and 219-449% for BC400 and BC700, respectively, whereas aging with Ca and Al had almost no effect on the mediating capacity (Fig. 6a & b) with similar mediated reduction rates of 0.82-1.73 $\times 10^{-3}\ h^{-1}$ and 2.11-3.58 $\times 10^{-3}\ h^{-1}$ for BC400 and BC700, respectively. It is noteworthy that BC400 had higher mediated reduction rate than BC700 after co-aging with either Fe(III) or Mn(II).

The increase of mediated reduction rate of aged biochar with Fe(III) and Mn(II) might be attributed to the valence transformation. As detected by XPS (Fig. 2), Fe(II), Mn(III) and Mn(IV) were formed on the biochar surface after the aging process, which would affect the electron mediation process. Fe(II) can mediate the lactate for Cr(VI) reduction through the formation of intermediate of Cr(V) during the electron transfer (Joe-Wong et al. 2017, Liu et al. 2019, Xu et al. 2020a), especially with the existence of organic acids due to the formation of Cr(V)−ligand complexes (e.g. Cr(V)-lactate) (Fendorf and Li 1996, Joe-Wong et al. 2017, Liu et al. 2019)

(Equations 8 and 9). As Cr(V) was unstable and had higher oxidation capacity, it would react easily with lactate and form Cr(III) (Equation 10). The increase of Fe(II) from 45.2% to 56.8% and from 39.6% to 40.4% was found after mediated reduction of Cr(VI) by 3-month aging of BC400 + Fe(III) and BC700 + Fe(III), respectively (Fig. 2), corroborating that Fe(II) on the mineral-biochar complexes assisted the electron mediation process. The amount of Fe(II) formation was the key to the mediated reduction rate of biochar aged with iron. BC400 produced more Fe(II) than BC700 (45.2-59.8% vs 39.3-39.6%, Fig. 2) after the aging process, and it also contained larger amount of Fe(II) after the mediated Cr(VI) reduction (56.8% > 40.4%), because of the higher electron donating capacity of BC400 (Table S1).Therefore, BC400 aged with Fe(III) gave higher mediated reduction rate than BC700 aged with Fe(III).

$$\text{Biochar}(e^-) + Fe^{3+} \rightarrow \text{Biochar} + Fe^{2+} \quad \text{Equation 8}$$

$$H^+ + CrO_4^{2-}(\text{Cr(VI)}) + Fe^{2+} \rightarrow HCrO_4^{2-}(\text{Cr(V)}) + Fe^{3+} \quad \text{Equation 9}$$

$$7H^+ + HCrO_4^{2-}(\text{Cr(V)}) + 2\text{Lactate}(e^-) \rightarrow Cr^{3+} + 2\text{Lactate} + 4H_2O \quad \text{Equation 10}$$

Similarly, Mn(III) formed on the aged biochar might reduce the Cr(VI) to Cr(V) through the valence transformation to Mn(IV) (Equations 11) and thus facilitated the Cr(VI) reduction with lactate (Equation 10). Besides, Mn(III) and Mn(IV) chelated with organic ligands often had a high oxidation capacity (Sun et al. 2015, Tian et al. 2019, Zhang et al. 2020, Zhong and Zhang 2020), which could directly act as an electron acceptor and generate radicals. The formation of free radicals (e.g. $O_2\cdot^-$) (Wu et al. 2021) or persistent radicals on the biochar (e.g. semi-

quinonyle-type radicals) (Xu et al. 2016) might act as an electron mediator, promoting the electron transfer process (Xu et al. 2019a). After the aging process, BC400 possessed more Mn(III) on the biochar surface than BC700 (28.3-29.7% > 25.3-26.1%, Fig. 2), while more Mn(IV) was formed on BC700 surface (15.3-20.2% > 11.9-17.8%, Fig. 2), due to the relatively lower electron accepting capacity of BC400 (Table S1). Meanwhile, BC400 showed a higher mediated reduction rates than BC700 after co-aging with Mn (11.8-14.9 $\times 10^{-3}\ h^{-1}$ > 7.63-8.01 $\times 10^{-3}\ h^{-1}$ Fig. 7), indicating the more important role of Mn(III) than Mn(IV) for the mediated reduction of Cr(VI).

$$H^{+} + CrO_4^{2-} + Mn(III) \rightarrow HCrO_4^{2-} + Mn(IV) \quad \text{Equation 11}$$

Compared with biochar aged alone, the presence of kaolinite caused no significant change of the mediated reduction rate (Table S3 and S4), while the increase of mediated reduction rate was found in the biochar aged with kaolinite + Fe(III) /Mn(II) (experimental setting 7-8) (Fig. 6c & 6d). Aging with kaolinite + Fe(III)/Mn(II) showed the mediated reduction rate constants of 4.15-12.5 $\times 10^{-3}\ h^{-1}$ and 1.59-3.56 $\times 10^{-3}\ h^{-1}$ for BC400 and BC700, respectively, which were far lower than the corresponding aging processes without kaolinite (11.8-20.3 $\times 10^{-3}\ h^{-1}$ for BC400 and 6.67-8.01$\times 10^{-3}\ h^{-1}$ for BC700). This might be attributed to lower concentrations of soluble Fe or Mn in the presence of kaolinite (Fig. S29-30 vs Fig. S24-25). Taking Fe as an example, only 19.8 mg L^{-1} total Fe was released into the solution from the biochar co-aged with kaolinite+ Fe(III) (Fig. S29), while the release amount of total Fe from the biochar co-aged with Fe(III) without kaolinite reached up to 43.9 mg L^{-1} (Fig. S24). Kaolinite can sorb mineral ions (Turan et al. 2007, Zhu et al. 2018) and

thus inhibit the mediating electron transfer process.

4. Conclusions and environmental implications

Our study demonstrated that, during the aging process, interactions with soil soluble mineral salts could reduce the surface –C-OH content, generate new minerals, and form biochar-mineral complexes on the biochar. Aging with soluble iron accelerated the oxidation of biochar to the maximum extent, while manganese inhibited this process due to the oxidation of Mn(II) to Mn(III) and Mn(IV). Interactions between mineral cations and biochar altered the redox activity of biochar for Cr(VI) reduction. The decrease of surface –C-OH after aging process was mainly responsible for the decline of biochars' direct electron donating capacity for Cr(VI). Meanwhile, aging without any minerals decreased the biochars' mediating capacity due to the decline of O-moieties, while co-aging with redox-active Fe(III) and Mn(II) facilitated the electron mediating process. Reductive formation of Fe(II) and oxidative formation of Mn(III) might be the key to the promotion of mediated reduction of Cr(VI). By contrast, the existence of kaolinite showed limited effects on the redox activity of biochar during the co-aging process with mineral ions.

In conclusion, the aging process could change the biochar's properties and redox activity, and the long-term interactions with minerals would further change the direct and indirect electron transfer processes. Therefore, biochar could hardly maintain the same redox capacity after the long-term aging process, but the existence of redox-active mineral ions, e.g., Mn and Fe, could facilitate the electron mediating process of

biochar and offset the loss of direct electron donating capacities. Considering the abundant mineral contents in the soil, it would be essential to further investigate this environmental factor during the aging process when applying biochar in field soil for environmental applications involving redox reactions, such as Cr(VI) reduction. More studies about impact of co-aging with soil moieties on biochar's redox activity for different application and quantitative analysis (e.g. electrochemical techniques) were recommended in the future.

Supporting Information

Supplementary data including 5 texts, 5 tables, and 32 figures related to this article can be found online.

Biochar characterization (Text S1); Electrochemical analysis of biochar (Text S2); Sampling and characterization method after Cr(VI) reduction (Text S3); XPS analysis and peak position (Text S4); Data analysis (Text S5); Physicochemical properties of biochar (Table S1); XPS results for the O1s binding state on the biochar surfaces after aging process (Table S2); Reduction rate constant of Cr(VI) by different biochar in different reaction system (Table S3-S4); XPS results for the O1s binding state on the aged biochar surfaces after Cr(VI) reduction with or without lactate (Table S5); XPS spectra of O1s for different aged biochar (Fig.S1-S2); FTIR patterns of biochar before and after reaction with Fe(III) (Fig. S3); XRD patterns of different aged biochar with kaolinite (Fig.S4); SEM for BC400 aged with iron or manganese for 3 months

(Fig.S5); SEM element mapping for different aged BC400 (Fig. S6); Change of Cr and metal concentration after addition of different aged biochar (Fig.S7-16); Cr proportion on the aged biochar after Cr(VI) removal with or without lactate as detected by XPS analysis (Fig.S17); SEM image of different 3-month aged BC400 after Cr reduction (Fig.S18); XPS spectra of O1s for different aged BC400 after Cr(VI) reduction with or without lactate (Fig.S19); SEM-element mapping of different 3-month aged BC400 after Cr reduction (Fig.S20); SEM-element mapping of different 3-month kaolinite co-aged BC400 before and after Cr(VI) reduction (Fig.S21); The reduction rate constant of Cr(VI) reduction by different aged BC400 and BC700 with lactate obtained from first-order reaction model (Fig.S22); Change of Cr and metal concentration after addition of different aged biochar with lactate (Fig.S23-S32).

Acknowledgement

This work was supported in part by National Natural Science Foundation of China (No. 21537002, 21777095, 42077112), National Key R&D Program of China (No. 2018YFC1802700, 2018YFC1800600), Science and Technology Commission of Shanghai Municipality (No. 20ZR1429100), and Hong Kong Research Grants Council (PolyU 15217818).

References

Archanjo, B.S., Mendoza, M.E., Albu, M., Mitchell, D.R.G., Hagemann, N., Mayrhofer, C., Mai, T.L.A., Weng, Z., Kappler, A., Behrens, S., Munroe, P., Achete, C.A., Donne, S., Araujo, J.R., van Zwieten, L., Horvat, J., Enders, A. and Joseph, S. (2017) Nanoscale analyses of the surface structure and composition of biochars extracted from field trials or after co-composting using advanced analytical electron microscopy. Geoderma 294, 70-79.

Arrigo, R., Haevecker, M., Wrabetz, S., Blume, R., Lerch, M., McGregor, J., Parrott, E.P.J., Zeitler, J.A., Gladden, L.F., Knop-Gericke, A., Schloegl, R. and Su, D.S. (2010) Tuning the Acid/Base Properties of Nanocarbons by Functionalization via Amination. Journal of the American Chemical Society 132(28), 9616-9630.

Bishop, M.E., Dong, H., Glasser, P., Briggs, B.R., Pentrak, M., Stucki, J.W., Boyanov, M.I., Kemner, K.M. and Kovarik, L. (2019) Reactivity of redox cycled Fe-bearing subsurface sediments towards hexavalent chromium reduction. Geochimica Et Cosmochimica Acta 252, 88-106.

Buerge, I.J. and Hug, S.J. (1999) Influence of Mineral Surfaces on Chromium(VI) Reduction by Iron(II). Environmental Science & Technology 33(23), 4285-4291.

Cao, X.D. and Harris, W. (2010) Properties of dairy-manure-derived biochar pertinent to its potential use in remediation. Bioresource technology 101(14), 5222-5228.

Cao, X.D., Ma, L.N., Liang, Y., Gao, B. and Harris, W. (2011) Simultaneous Immobilization of Lead and Atrazine in Contaminated Soils Using Dairy-Manure Biochar. Environmental Science & Technology 45(11), 4884-4889.

Chen, Y.-d., Bai, S., Li, R., Su, G., Duan, X., Wang, S., Ren, N.-q. and Ho, S.-H. (2019) Magnetic biochar catalysts from anaerobic digested sludge: Production, application and environment impact. Environment International 126, 302-308.

Deng, B., Lan, L., Houston, K. and Brady, P.V. (2003) Effects of Clay Minerals on Cr(VI) Reduction by Organic Compounds. Environmental Monitoring and Assessment 84(1), 5-18.

Deng, Y., Huang, S., Dong, C., Meng, Z. and Wang, X. (2020) Competitive adsorption behaviour and mechanisms of cadmium, nickel and ammonium from aqueous solution by fresh and ageing rice straw biochars. Bioresource technology 303, 122853.

Fendorf, S.E. and Li, G. (1996) Kinetics of Chromate Reduction by Ferrous Iron. Environmental Science & Technology 30(5), 1614-1617.

Gehling, W. and Dellinger, B. (2013) Environmentally Persistent Free Radicals and Their Lifetimes in PM2.5. Environmental Science & Technology 47(15), 8172-8178.

Ghaffar, A., Ghosh, S., Li, F.F., Dong, X.D., Zhang, D., Wu, M., Li, H. and Pan, B. (2015) Effect of biochar aging on surface characteristics and adsorption behavior of dialkyl phthalates. Environmental Pollution 206, 502-509.

Guo, Y., Tang, W., Wu, J.G., Huang, Z.Q. and Dai, J.Y. (2014) Mechanism of Cu(II) adsorption inhibition on biochar by its aging process. Journal of Environmental Sciences 26(10), 2123-2130.

Han, Y.T., Cao, X., Ouyang, X., Sohi, S.P. and Chen, J.W. (2016) Adsorption kinetics of magnetic biochar derived from peanut hull on removal of Cr (VI) from aqueous solution: Effects of production conditions and particle size. Chemosphere 145, 336-341.

Huang, Z., Hu, L., Tang, W., Guo, Y. and Dai, J. (2020) Effects of biochar aging on adsorption

behavior of phenanthrene. Chemical Physics Letters 759, 137948.
Hussain, M., Farooq, M., Nawaz, A., Al-Sadi, A.M., Solaiman, Z.M., Alghamdi, S.S., Ammara, U., Ok, Y.S. and Siddique, K.H.M. (2017) Biochar for crop production: potential benefits and risks. Journal of Soils and Sediments 17(3), 685-716.
Inoué, S., Yasuhara, A., Ai, H., Hochella, M.F. and Murayama, M. (2019) Mn(II) oxidation catalyzed by nanohematite surfaces and manganite/hausmannite core-shell nanowire formation by self-catalytic reaction. Geochimica Et Cosmochimica Acta 258, 79-96.
Joe-Wong, C., Brown, G.E. and Maher, K. (2017) Kinetics and Products of Chromium(VI) Reduction by Iron(II/III)-Bearing Clay Minerals. Environmental Science & Technology 51(17), 9817-9825.
Jones, D.L. (1998) Organic acids in the rhizosphere – a critical review. Plant And Soil 205(1), 25-44.
Krishnamurti, G.S.R., Cieslinski, G., Huang, P.M. and VanRees, K.C.J. (1997) Kinetics of cadmium release from soils as influenced by organic acids: Implication in cadmium availability. Journal of Environmental Quality 26(1), 271-277.
Kwak, S., Yoo, J.-C., Moon, D.H. and Baek, K. (2018) Role of clay minerals on reduction of Cr(VI). Geoderma 312, 1-5.
Lehmann, J. (2007) A handful of carbon. Nature 447(7141), 143-144.
Li, F.Y., Cao, X.D., Zhao, L., Yang, F., Wang, J.F. and Wang, S.W. (2013) Short-term effects of raw rice straw and its derived biochar on greenhouse gas emission in five typical soils in China. Soil Science and Plant Nutrition 59(5), 800-811.
Li, S., Shao, L., Zhang, H., He, P. and Lü, F. (2020) Quantifying the Contributions of Surface Area and Redox-active Moieties to Electron Exchange Capacities of Biochar. Journal of Hazardous Materials, 122541.
Lin, Y., Munroe, P., Joseph, S., Kimber, S. and Zwieten, L.V. (2012) Nanoscale organo-mineral reactions of biochars in ferrosol: an investigation using microscopy. Plant & Soil 357(1-2), 369-380.
Liu, P., Ptacek, C.J., Blowes, D.W., Finfrock, Y.Z. and Liu, Y. (2020) Characterization of chromium species and distribution during Cr(VI) removal by biochar using confocal micro-X-ray fluorescence redox mapping and X-ray absorption spectroscopy. Environment International 134, 105216.
Liu, X., Dong, H., Zeng, Q., Yang, X. and Zhang, D. (2019) Synergistic Effects of Reduced Nontronite and Organic Ligands on Cr(VI) Reduction. Environmental Science & Technology 53(23), 13732-13741.
Luo, Y., Tan, W., Suib, S.L., Qiu, G. and Liu, F. (2020) Epitaxial growth mechanism of heterogeneous catalytic oxidation of Mn(II) on manganite under oxic conditions. Chemical Geology 547, 119670.
Mandal, S., Sarkar, B., Bolan, N., Ok, Y.S. and Naidu, R. (2017) Enhancement of chromate reduction in soils by surface modified biochar. Journal of Environmental Management 186, 277-284.
Mia, S., Dijkstra, F.A. and Singh, B. (2017) Advances in Agronomy, Vol 141. Sparks, D.L. (ed), pp. 1-51, Elsevier Academic Press Inc, San Diego.
Mukherjee, A., Zimmerman, A.R., Hamdan, R. and Cooper, W.T. (2014) Physicochemical changes in pyrogenic organic matter (biochar) after 15 months of field aging. Solid Earth

5(2), 693-704
Morgan, J.J. (2005) Kinetics of reaction between O2 and Mn(II) species in aqueous solutions. Geochimica Et Cosmochimica Acta 69(1), 35-48..
Mullet, M., Demoisson, F., Humbert, B., Michot, L.J. and Vantelon, D. (2007) Aqueous Cr(VI) reduction by pyrite: Speciation and characterisation of the solid phases by X-ray photoelectron, Raman and X-ray absorption spectroscopies. Geochimica Et Cosmochimica Acta 71(13), 3257-3271.
Mumme, J., Getz, J., Prasad, M., Lüder, U., Kern, J., Mašek, O. and Buss, W. (2018) Toxicity screening of biochar-mineral composites using germination tests. Chemosphere 207, 91-100.
Nelson, J., Joe-Wong, C. and Maher, K. (2019) Cr(VI) reduction by Fe(II) sorbed to silica surfaces. Chemosphere 234, 98-107.
Odinga, E.S., Waigi, M.G., Gudda, F.O., Wang, J., Yang, B., Hu, X., Li, S. and Gao, Y. (2020) Occurrence, formation, environmental fate and risks of environmentally persistent free radicals in biochars. Environment International 134, 105172.
Qi, F.J., Kuppusamy, S., Naidu, R., Bolan, N.S., Ok, Y.S., Lamb, D., Li, Y.B., Yu, L.B., Semple, K.T. and Wang, H.L. (2017) Pyrogenic carbon and its role in contaminant immobilization in soils. Critical Reviews in Environmental Science and Technology 47(10), 795-876.
Qin, C., Wang, H., Yuan, X., Xiong, T., Zhang, J. and Zhang, J. (2020) Understanding structure-performance correlation of biochar materials in environmental remediation and electrochemical devices. Chemical Engineering Journal 382, 122977.
Qiu, Y., Xu, X., Xu, Z., Liang, J., Yu, Y. and Cao, X. (2020) Contribution of different iron species in the iron-biochar composites to sorption and degradation of two dyes with varying properties. Chemical Engineering Journal 389, 124471.
Rafique, M., Ortas, I., Rizwan, M., Chaudhary, H.J., Gurmani, A.R. and Hussain Munis, M.F. (2020) Residual effects of biochar and phosphorus on growth and nutrient accumulation by maize (Zea mays L.) amended with microbes in texturally different soils. Chemosphere 238, 124710.
Rajapaksha, A.U., Alam, M.S., Chen, N., Alessi, D.S., Igalavithana, A.D., Tsang, D.C.W. and Ok, Y.S. (2018) Removal of hexavalent chromium in aqueous solutions using biochar: Chemical and spectroscopic investigations. Science of the Total Environment 625, 1567-1573.
Rechberger, M.V., Kloss, S., Rennhofer, H., Tintner, J., Watzinger, A., Soja, G., Lichtenegger, H. and Zehetner, F. (2017) Changes in biochar physical and chemical properties: Accelerated biochar aging in an acidic soil. Carbon 115, 209-219.
Ren, X.H., Wang, F., Zhang, P., Guo, J.K. and Sun, H.W. (2018) Aging effect of minerals on biochar properties and sorption capacities for atrazine and phenanthrene. Chemosphere 206, 51-58.
Schmidt, H.P., Anca-Couce, A., Hagemann, N., Werner, C., Gerten, D., Lucht, W. and Kammann, C. (2019) Pyrogenic carbon capture and storage. Global Change Biology Bioenergy 11(4), 573-591.
Shi, J., McGill, W.B., Chen, N., Rutherford, P.M., Whitcombe, T.W. and Zhang, W. (2020) Formation and Immobilization of Cr(VI) Species in Long-Term Tannery Waste Contaminated Soils. Environmental Science & Technology 54(12), 7226-7235.

Sigg, L. and Stumm, W. (1981) The interaction of anions and weak acids with the hydrous goethite (α-FeOOH) surface. Colloids and Surfaces 2(2), 101-117.
Singh, B., Fang, Y., Cowie, B.C.C. and Thomsen, L. (2014) NEXAFS and XPS characterisation of carbon functional groups of fresh and aged biochars. Organic Geochemistry 77, 1-10.
Sun, B., Guan, X., Fang, J. and Tratnyek, P.G. (2015) Activation of Manganese Oxidants with Bisulfite for Enhanced Oxidation of Organic Contaminants: The Involvement of Mn(III). Environmental Science & Technology 49(20), 12414-12421.
Sun, T., Levin, B.D.A., Guzman, J.J.L., Enders, A., Muller, D.A., Angenent, L.T. and Lehmann, J. (2017) Rapid electron transfer by the carbon matrix in natural pyrogenic carbon. Nature Communications 8.
Sun, Y., Yu, I.K.M., Tsang, D.C.W., Cao, X., Lin, D., Wang, L., Graham, N.J.D., Alessi, D.S., Komárek, M., Ok, Y.S., Feng, Y. and Li, X.-D. (2019) Multifunctional iron-biochar composites for the removal of potentially toxic elements, inherent cations, and hetero-chloride from hydraulic fracturing wastewater. Environment International 124, 521-532.
Tan, L., Ma, Z., Yang, K., Cui, Q., Wang, K., Wang, T., Wu, G.-L. and Zheng, J. (2020) Effect of three artificial aging techniques on physicochemical properties and Pb adsorption capacities of different biochars. Science of the Total Environment 699, 134223.
Tian, S.-Q., Wang, L., Liu, Y.-L., Yang, T., Huang, Z.-S., Wang, X.-S., He, H.-Y., Jiang, J. and Ma, J. (2019) Enhanced Permanganate Oxidation of Sulfamethoxazole and Removal of Dissolved Organics with Biochar: Formation of Highly Oxidative Manganese Intermediate Species and in Situ Activation of Biochar. Environmental Science & Technology 53(9), 5282-5291.
Tu, C., Wei, J., Guan, F., Liu, Y., Sun, Y. and Luo, Y. (2020) Biochar and bacteria inoculated biochar enhanced Cd and Cu immobilization and enzymatic activity in a polluted soil. Environment International 137, 105576.
Turan, P., Doğan, M. and Alkan, M. (2007) Uptake of trivalent chromium ions from aqueous solutions using kaolinite. Journal of Hazardous Materials 148(1), 56-63.
Wan, Z., Cho, D.-W., Tsang, D.C.W., Li, M., Sun, T. and Verpoort, F. (2019) Concurrent adsorption and micro-electrolysis of Cr(VI) by nanoscale zerovalent iron/biochar/Ca-alginate composite. Environmental Pollution 247, 410-420.
Wan, Z., Sun, Y., Tsang, D.C.W., Xu, Z., Khan, E., Liu, S.-H. and Cao, X. (2020) Sustainable impact of tartaric acid as electron shuttle on hierarchical iron-incorporated biochar. Chemical Engineering Journal 395, 125138.
Wang, D.J., Zhang, W. and Zhou, D.M. (2013) Antagonistic Effects of Humic Acid and Iron Oxyhydroxide Grain-Coating on Biochar Nanoparticle Transport in Saturated Sand. Environmental Science & Technology 47(10), 5154-5161.
Wang, L., O'Connor, D., Rinklebe, J., Ok, Y.S., Tsang, D.C.W., Shen, Z. and Hou, D. (2020) Biochar Aging: Mechanisms, Physicochemical Changes, Assessment, And Implications for Field Applications. Environmental Science & Technology 54(23), 14797-14814.
Wu, K., Wang, M., Li, A., Zhao, Z., Liu, T., Hao, X., Yang, S. and Jin, P. (2021) The enhanced As(III) removal by Fe-Mn-Cu ternary oxide via synergistic oxidation: Performances and mechanisms. Chemical Engineering Journal 406, 126739.
Xiao, X., Chen, B.L., Chen, Z.M., Zhu, L.Z. and Schnoor, J.L. (2018) Insight into Multiple

and Multilevel Structures of Biochars and Their Potential Environmental Applications: A Critical Review. Environmental Science & Technology 52(9), 5027-5047.
Xu, J., Yin, Y., Tan, Z., Wang, B., Guo, X., Li, X. and Liu, J. (2018a) Enhanced removal of Cr(VI) by biochar with Fe as electron shuttles. Journal of Environmental Sciences.
Xu, S., Adhikari, D., Huang, R., Zhang, H., Tang, Y., Roden, E. and Yang, Y. (2016) Biochar-Facilitated Microbial Reduction of Hematite. Environmental Science & Technology 50(5), 2389-2395.
Xu, X., Huang, H., Zhang, Y., Xu, Z. and Cao, X. (2019a) Biochar as both electron donor and electron shuttle for the reduction transformation of Cr(VI) during its sorption. Environ Pollut 244, 423-430.
Xu, Z., Xu, X., Tao, X., Yao, C., Tsang, D.C.W. and Cao, X. (2019b) Interaction with low molecular weight organic acids affects the electron shuttling of biochar for Cr(VI) reduction. Journal of Hazardous Materials 378.
Xu, Z., Xu, X., Tsang, D.C.W. and Cao, X. (2018b) Contrasting impacts of pre- and post-application aging of biochar on the immobilization of Cd in contaminated soils. Environmental Pollution 242, 1362-1370.
Xu, Z., Xu, X., Tsang, D.C.W., Yang, F., Zhao, L., Qiu, H. and Cao, X. (2020a) Participation of soil active components in the reduction of Cr(VI) by biochar: Differing effects of iron mineral alone and its combination with organic acid. Journal of Hazardous Materials 384, 121455.
Xu, Z., Xu, X., Zhang, Y., Yu, Y. and Cao, X. (2020b) Pyrolysis-temperature depended electron donating and mediating mechanisms of biochar for Cr(VI) reduction. Journal of Hazardous Materials 388, 121794.
Yang, F., Xu, Z., Yu, L., Gao, B., Xu, X., Zhao, L. and Cao, X. (2018) Kaolinite Enhances the Stability of the Dissolvable and Undissolvable Fractions of Biochar via Different Mechanisms. Environmental Science & Technology 52(15), 8321-8329.
Yang, F., Zhao, L., Gao, B., Xu, X.Y. and Cao, X.D. (2016) The Interfacial Behavior between Biochar and Soil Minerals and Its Effect on Biochar Stability. Environmental Science & Technology 50(5), 2264-2271.
Yu, I.K.M., Tsang, D.C.W., Yip, A.C.K., Chen, S.S., Ok, Y.S. and Poon, C.S. (2016) Valorization of food waste into hydroxymethylfurfural: Dual role of metal ions in successive conversion steps. Bioresource technology 219, 338-347.
Yu, Z., Chen, H.Y.H., Searle, E.B., Sardans, J., Ciais, P., Peñuelas, J. and Huang, Z. (2020) Whole soil acidification and base cation reduction across subtropical China. Geoderma 361, 114107.
Zhang, J., Zhao, W., Wu, S., Yin, R. and Zhu, M. (2020) Surface dual redox cycles of Mn(III)/Mn(IV) and Cu(I)/Cu(II) for heterogeneous peroxymonosulfate activation to degrade diclofenac: Performance, mechanism and toxicity assessment. Journal Of Hazardous Materials, 124623.
Zhang, Y., Xu, X., Cao, L., Ok, Y.S. and Cao, X. (2018) Characterization and quantification of electron donating capacity and its structure dependence in biochar derived from three waste biomasses. Chemosphere 211, 1073-1081.
Zhang, Y., Xu, X., Zhang, P., Ling, Z., Qiu, H. and Cao, X. (2019) Pyrolysis-temperature depended quinone and carbonyl groups as the electron accepting sites in barley grass derived

biochar. Chemosphere 232, 273-280.
Zhao, L., Cao, X.D., Masek, O. and Zimmerman, A. (2013) Heterogeneity of biochar properties as a function of feedstock sources and production temperatures. Journal Of Hazardous Materials 256, 1-9.
Zhao, N., Zhao, C., Tsang, D.C.W., Liu, K., Zhu, L., Zhang, W., Zhang, J., Tang, Y. and Qiu, R. (2021) Microscopic mechanism about the selective adsorption of Cr(VI) from salt solution on O-rich and N-rich biochars. Journal of Hazardous Materials 404, 124162.
Zhao, X., Zhong, X., Bao, H., Li, H., Li, G., Tuo, D., Lin, Q. and Brookes, P.C. (2007) Relating soil P concentrations at which P movement occurs to soil properties in Chinese agricultural soils. Geoderma 142(3), 237-244.
Zhao, Z. and Zhou, W. (2019) Insight into interaction between biochar and soil minerals in changing biochar properties and adsorption capacities for sulfamethoxazole. Environmental Pollution 245, 208-217.
Zhong, D., Zhang, Y., Wang, L., Chen, J., Jiang, Y., Tsang, D.C.W., Zhao, Z., Ren, S., Liu, Z. and Crittenden, J.C. (2018) Mechanistic insights into adsorption and reduction of hexavalent chromium from water using magnetic biochar composite: Key roles of Fe3O4 and persistent free radicals. Environmental Pollution 243, 1302-1309.
Zhong, S. and Zhang, H. (2020) Mn(III)-ligand complexes as a catalyst in ligand-assisted oxidation of substituted phenols by permanganate in aqueous solution. Journal of Hazardous Materials 384, 121401.
Zhu, H., Xiao, X., Guo, Z., Han, X., Liang, Y., Zhang, Y. and Zhou, C. (2018) Adsorption of vanadium (V) on natural kaolinite and montmorillonite: Characteristics and mechanism. Applied Clay Science 161, 310-316.

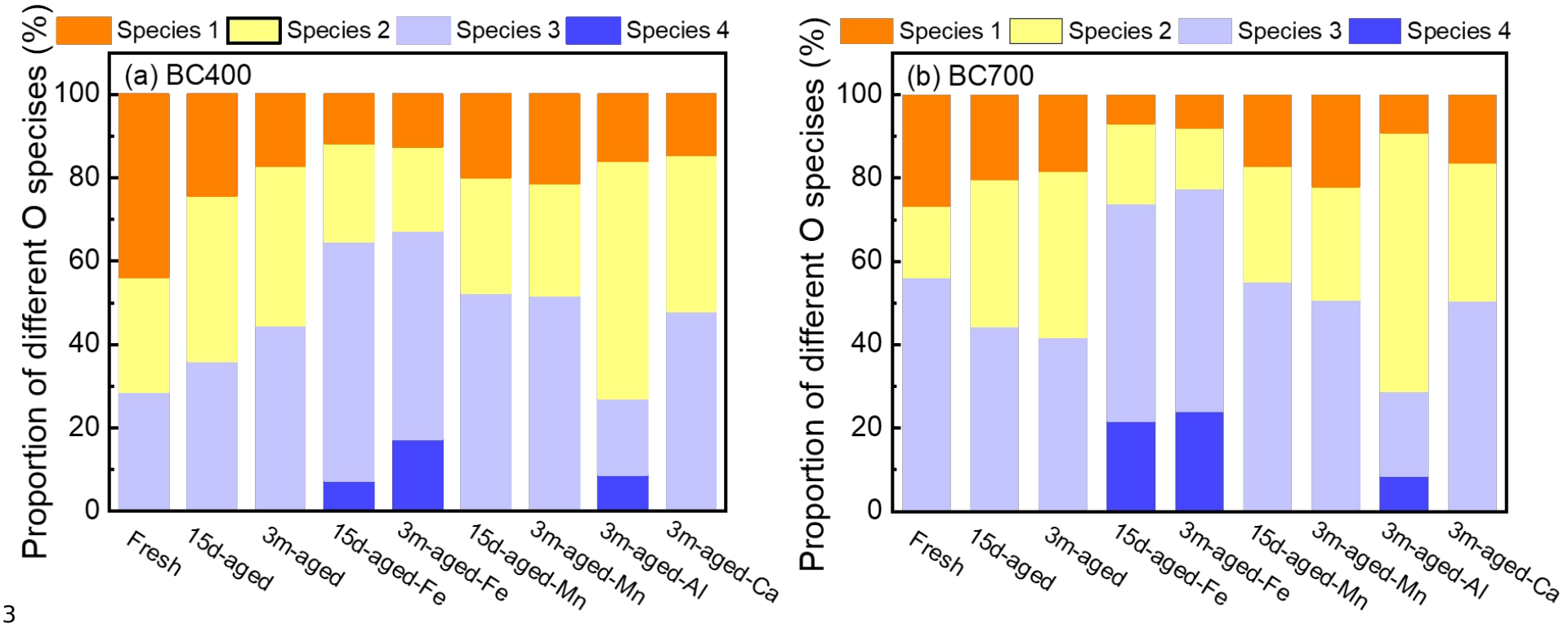

773

774Figure 1 Changes of biochar surface O-moieties after the 15-day and 3-month aging with different soil minerals as detected by XPS (a: BC400;
775b: BC700) (Species 1: -C-OH; Species 2: C-OC; Species 3: -O-C=O; Species 4: quinonyl -C=O) (XPS results were shown in Fig.S1 & S2 and
776Table S2)

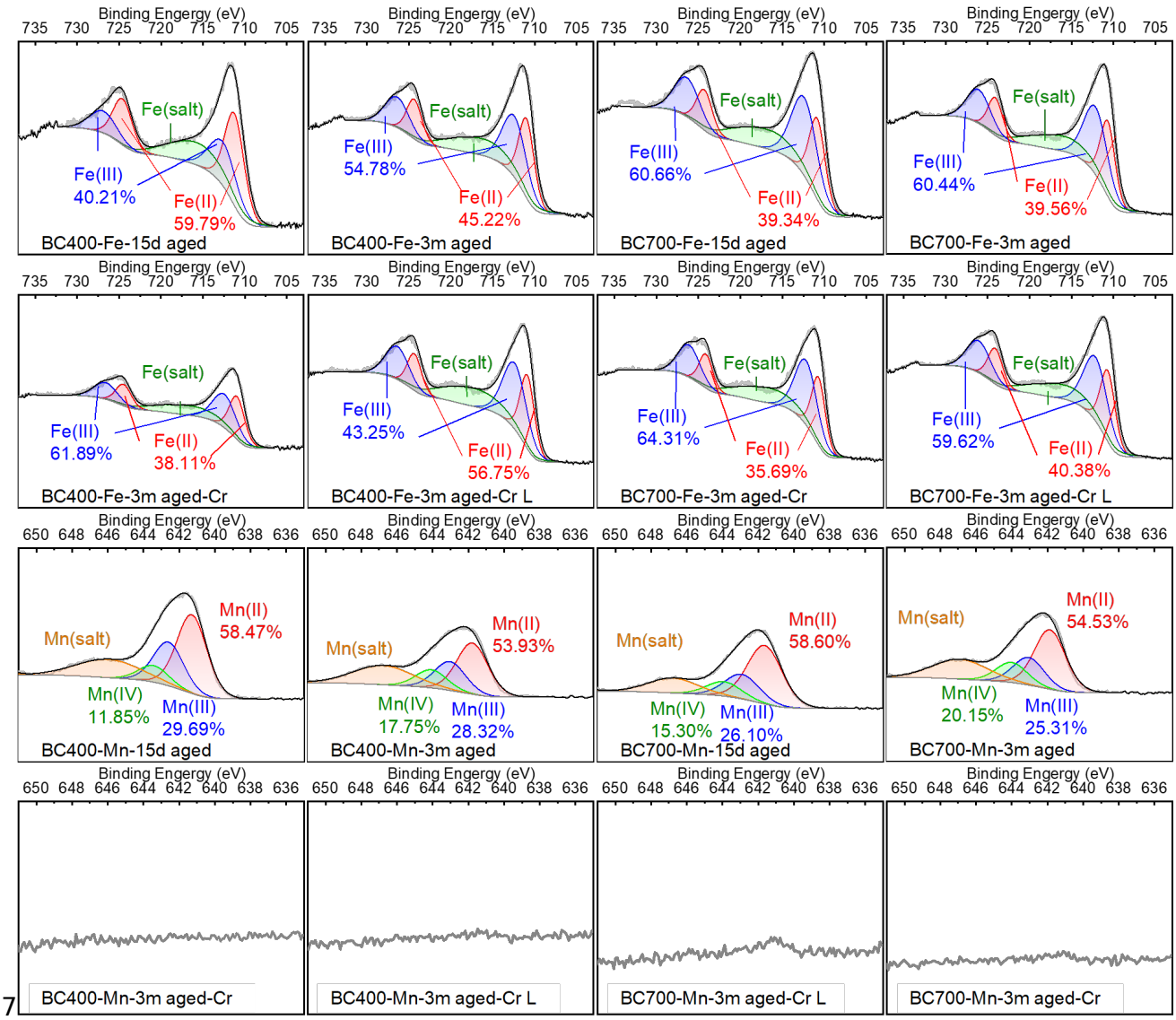

777

778Figure 2 XPS spectra of high-resolution scan of Fe 2p and Mn 2p for different aged
779BC400 and BC700 before and after Cr(VI) removal with or without lactate (Cr: after
780Cr removal without lactate; Cr-L: after Cr removal with lactate)

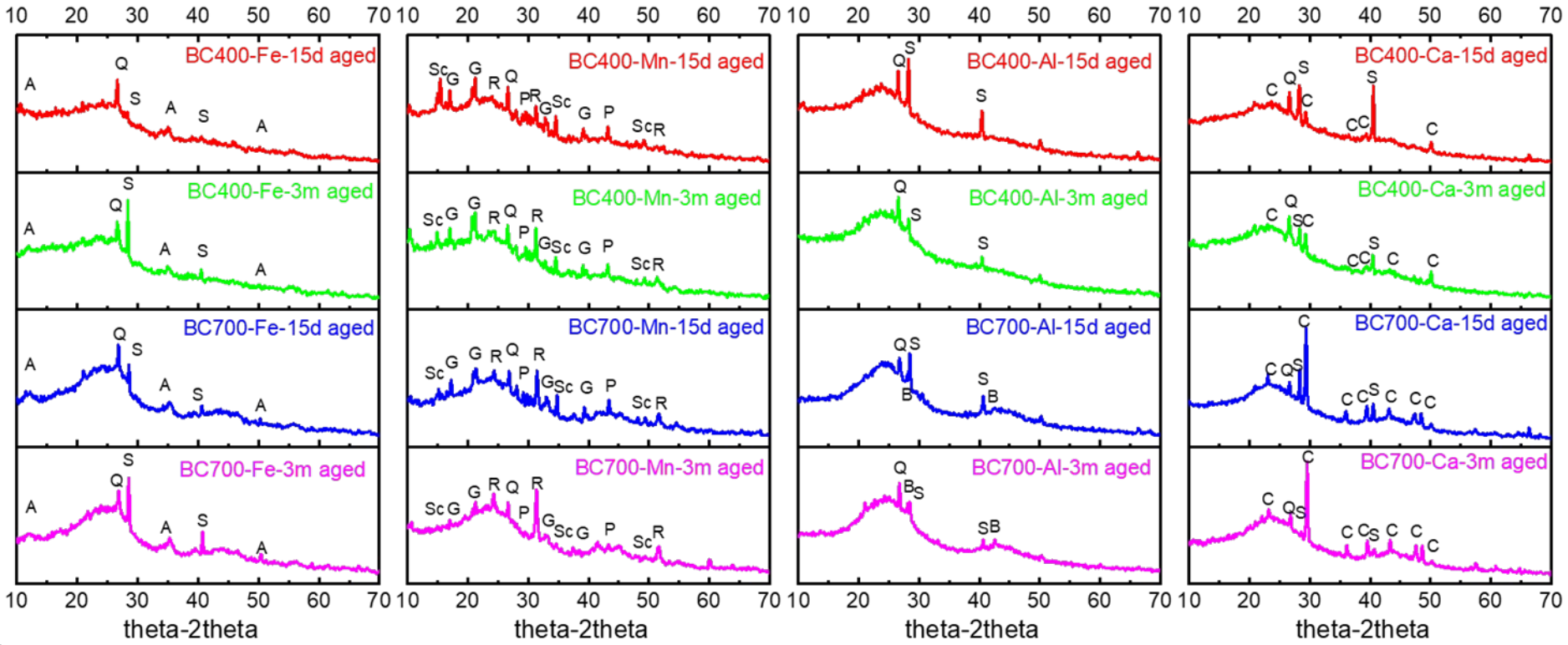

781

782Figure 3 XRD patterns of different aged biochar. (A: Akaganeite-Q β-FeOOH; Q: Quartz SiO_2, S: Sylvite KCl; Sc: Scacchite $MnCl_2$; R:
783Rhodochrosite $MnCO_3$; P: Potassium Manganese Oxide K_2MnO_3; G: Groutite MnOOH; B: Boehmite AlOOH; C: Calcite $CaCO_3$)
784

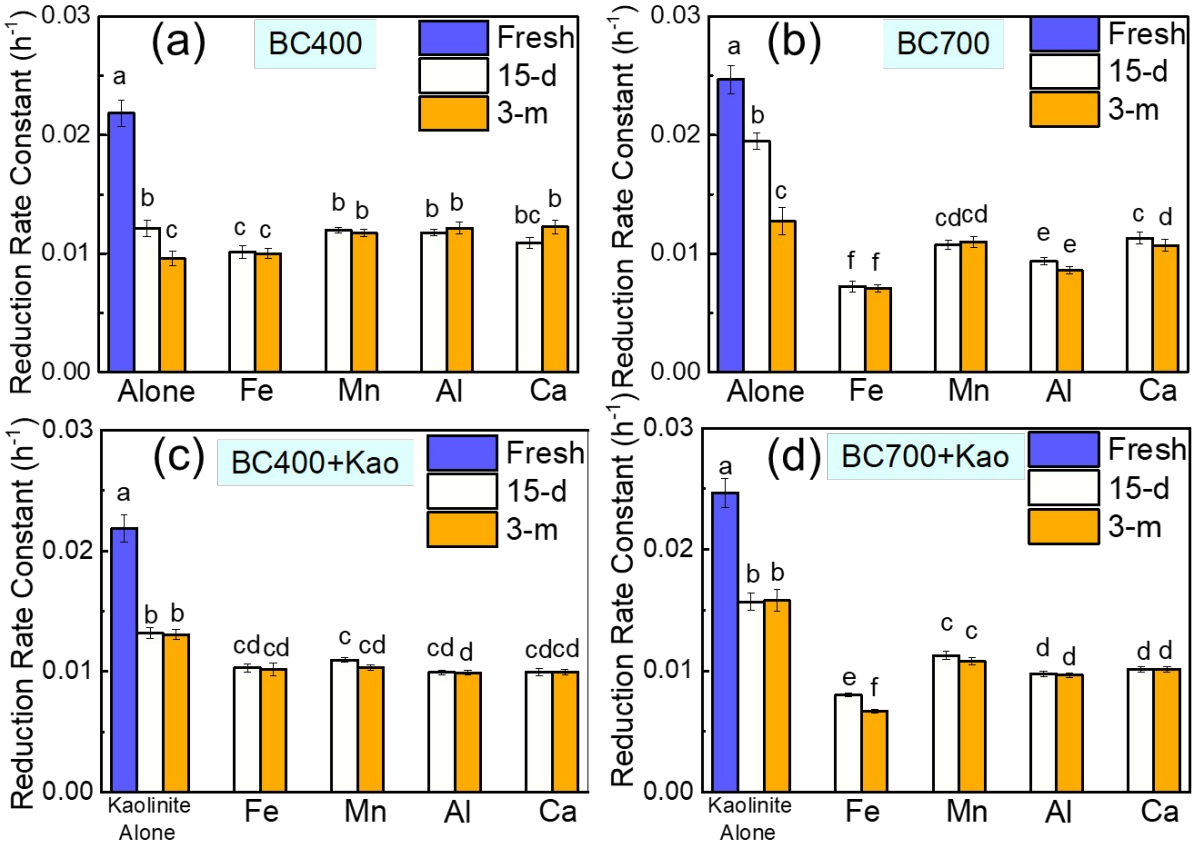

785

786Figure 4 The reduction rate constants of Cr(VI) reduction by different aged BC400 and BC700 alone obtained from first-order reaction model (a:
787BC400 aged with mineral ions alone; b: BC700 aged with mineral ions alone; c: BC400 aged with kaolinite and other mineral ions; d: BC700
788aged with kaolinite and other mineral ions) (error bars come from the triplicate repeat; mean values in each experiment followed by the same
789letters are not significantly different using Tukey's HSD test at $p < 0.05$) (Data and kinetics results were shown in Fig.S7-16 and Table S3-4)

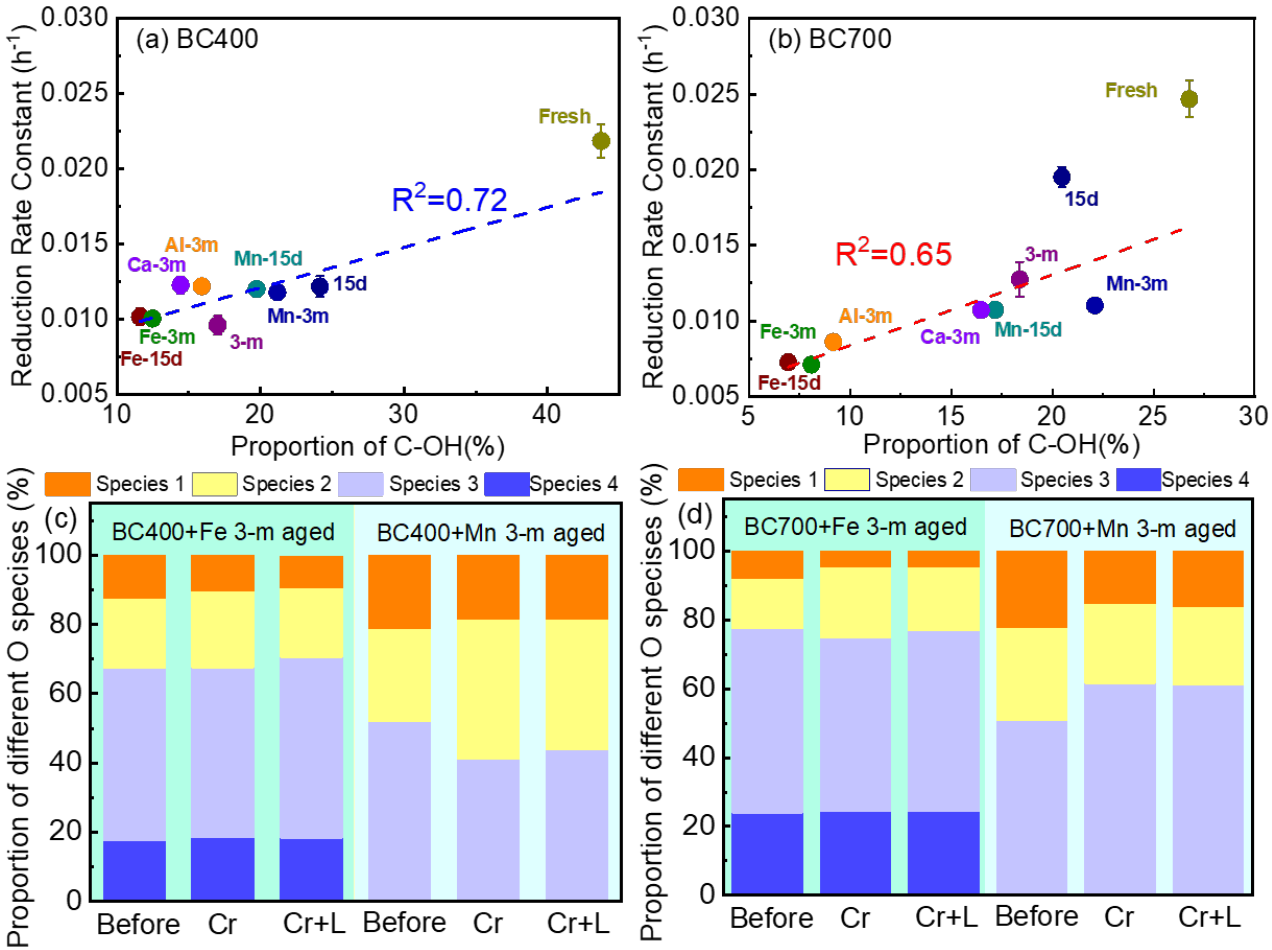

790

791Figure 5 Relationship between reduction rate and –C-OH proportion of BC400(a) and BC700(b); Changes of surface O-content before and after
792the Cr(VI) reduction process for different aged BC400(d) and BC700(d) (Species 1: -C-OH; Species 2: C-OC; Species 3: -O-C=O; Species 4:
793quinonyl -C=O) (XPS results were shown in Fig.S1-2, S20 and Table S1, S5)

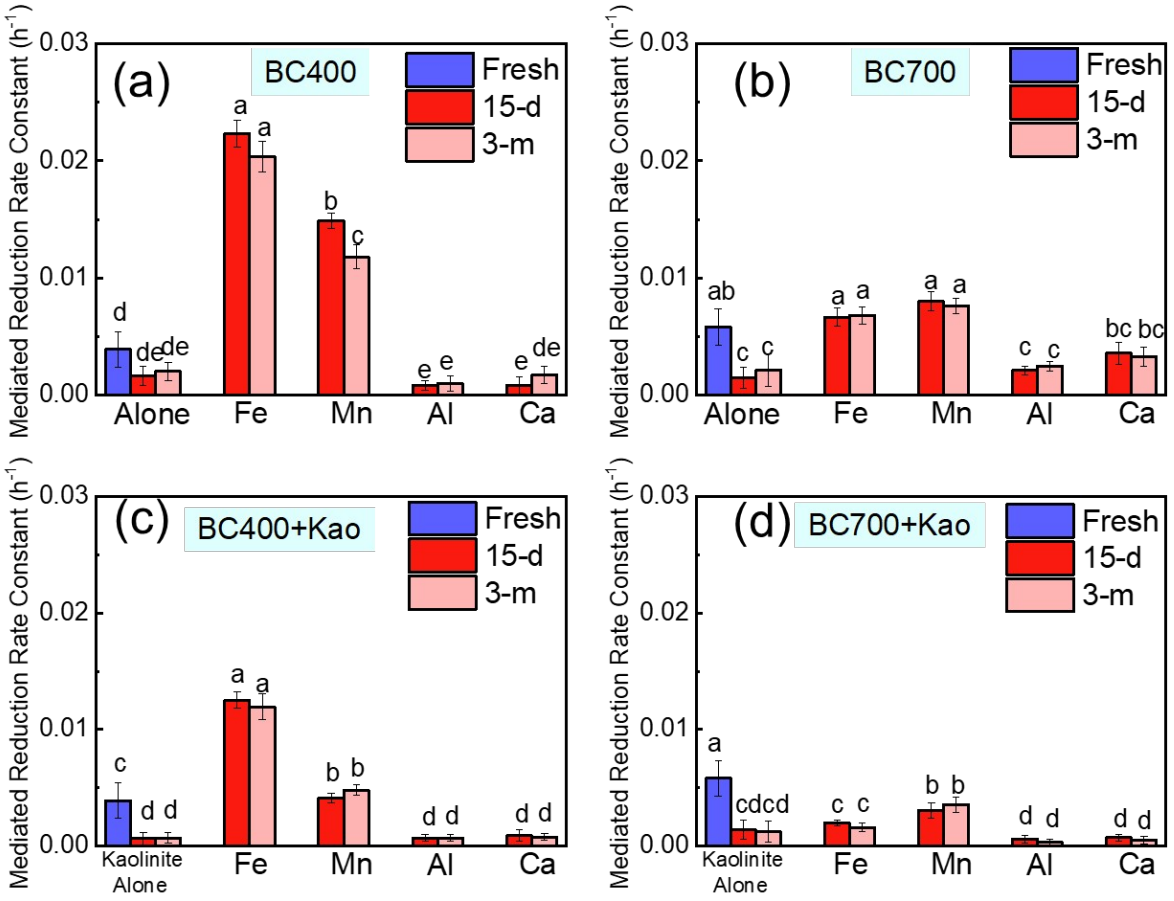

794

795Figure 6 The mediated reduction rate constants of Cr(VI) reduction by different aged BC400 and BC700 with lactate (a: BC400 aged with
796mineral ions alone; b: BC700 aged with mineral ions alone; c: BC400 aged with kaolinite and other mineral ions; d: BC700 aged with kaolinite
797and other mineral ions) (error bar comes from the triplicate repeat, Mean values in each experiment followed by the same letters are not
798significantly different using Tukey's HSD test at $p < 0.05$) (Data and kinetics results were shown in Fig.S23-32 and Table S3-S4)